DEMONSTRATION AND ANALYSIS OF THE PHOTOCURRENT PRODUCED BY ABSORPTION OF TWO SUB-BANDGAP PHOTONS IN A QUANTUM DOT INTERMEDIATE BAND SOLAR CELL

E. Antolín*, A. Martí, P. G. Linares, E. Cánovas, D. Fuertes Marrón and A. Luque
Instituto de Energía Solar – ETSIT, Universidad Politécnica de Madrid, Ciudad Universitaria sn, 28040 Madrid, Spain
*Phone: +34 914533549, FAX: +34 915446341, email: elisa@ies-def.upm.es

C. D. Farmer and C. R. Stanley
Department of Electronics and Electrical Engineering, University of Glasgow, Glasgow G12 8QQ, U.K.

ABSTRACT: In order to surpass the efficiency limit of single gap solar cells, intermediate band solar cells (IBSC) have to fulfill two requirements: the production of extra photocurrent by absorption of sub-bandgap photons in electronic transitions involving the intermediate band (IB) and the preservation of a high output voltage, not limited by the existence of this band. This work presents experimental evidence of the production of electron-hole pairs by absorption of two sub-bandgap photons in IBSC prototypes fabricated with InAs/GaAs QD material. The experiments were carried out at low temperatures using a specifically designed modulated photocurrent measurement set-up with two light beams. The results are analysed with the help of a simple equivalent circuit model. This analysis is also used to highlight the relevance of the two-photon mechanism demonstrated in the experiment. It is discussed that, although the absorption of sub-bandgap photons in one of the IB transitions and subsequent thermal escape of carriers is a sufficient mechanism to obtain a photocurrent enhancement, the absorption of sub-bandgap photons in *both* transitions involving the IB is a requisite for the voltage preservation in IBSCs.
Keywords: High Efficiency; Intermediate Band; Quantum Dots.

1 INTRODUCTION

It is well-known that the efficiency achievable by conventional solar cells is fundamentally limited by the impossibility of fully converting through a discrete bandgap transition the energy distributed in a continuous photon spectrum. Detailed balance calculations set 40.7% as the fundamental efficiency limit for single gap conversion, where photons of higher energy than the bandgap are not efficiently used and those with energy lower than that threshold are wasted. This limit can be surpassed by a photovoltaic device which combines different absorption thresholds, such as multi-junction solar cells, which are presently showing a rapid increase in efficiency records. The intermediate band solar cell (IBSC) constitutes an alternative concept for combining different absorption thresholds in one photovoltaic device, with an efficiency limit (63.2%) similar to that of a three-junction cell, but in a more compact design [1].

The high efficiency limit of the IBSC relays on the production of extra photocurrent by the simultaneous absorption of sub-bandgap photons in two different electronic transitions allowed by the existence of an intermediate band (IB). These two transitions constitute the two lower absorption thresholds that, added to the fundamental bandgap of the semiconductor, make the potential of this system equivalent to that of a three-junction cell. But in principle it is also possible to obtain extra photocurrent in an IBSC device using only one of the two low energy transitions. One of the objectives of this paper will be to analyze the consequences on the global performance of the IBSC of using only one sub-bandgap transition.

The design of an IBSC, as well as its implementation by means of quantum dot (QD) materials, have been described in previous works (see for instance [1, 2]). For that reason, here we will focus on the characteristics of state-of-the-art QD-IBSC prototypes in comparison to the IBSC theoretical model, rather than extending on the details of the model itself.

The IBSC design is based on the use of an IB material, characterized by the existence of an isolated electronic band between the conduction and valence bands (CB and VB, respectively). In the QD-IBSC used in this work, the IB is formed by the confined states introduced by an array of InAs QDs embedded in a GaAs matrix. The IB divides the main semiconductor bandgap E_G (in our case that of GaAs, 1.4 eV at room temperature) in two sub-bandgaps, referred to as E_L (the smallest one, in our case that between IB and CB) and E_H (the complementary of the later, in our case between VB and IB). Thus, we have three possible optical transitions in the IB material, that we label T_{VC}, T_{VI} and T_{IC} (transitions in which an electron is promoted from the VB to the CB, from the VB to the IB and from the IB to the CB, respectively). Through modulated doping of the QDs we semi-fill the IB with electrons, in order to enable the simultaneous occurrence of both T_{VI} and T_{IC}. In other words, we locate the Fermi level under equilibrium conditions at the energy position of the IB.

In an IBSC the IB material is sandwiched between two emitters of conventional semiconductor of opposite doping, which in our cells are also made of GaAs. They act as selective contacts, pinning the quasi-Fermi levels of electrons (E_{Fe}) and holes (E_{Fh}) when the cell is in operation. Consequently, the output voltage of the cell, given by the separation between both quasi-Fermi levels, is preserved, i.e. it is only limited by E_G. On the other hand, the IB is isolated from the contacts. While absorption of high energy photons in T_{VC} contributes directly to the photocurrent flow that takes place in the CB and VB, sub-bandgap photons contribute through a two-step mechanism: an electron-hole pair is created when two sub-bandgap photons are absorbed, one in T_{VI} and the other in T_{IC}. The electronic population of the IB is described by a third quasi-Fermi level (E_{FIB}). At this point it must be remarked that the "absorption of two photons" that will be discussed throughout the paper does not refer to the simultaneous absorption of two photons by a single electron in the IB, a rather unlikely three particle collision mechanism. Thanks to the existence of the three bands and the associated three quasi-Fermi levels, the interchange of carriers between bands is governed by analogous statistical laws as in a two-band semiconductor.

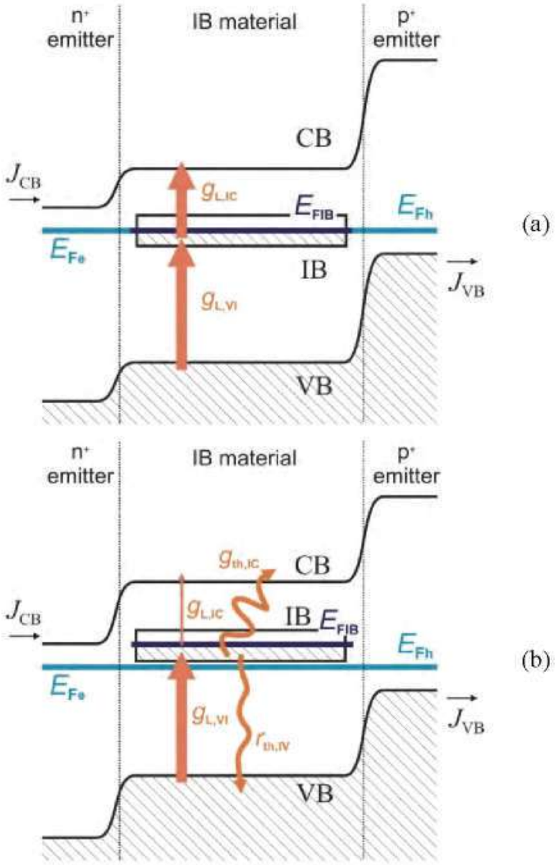

Fig. 1: Two possible band diagrams for an IBSC when it is short-circuited and illuminated only with sub-bandgap photons. Light generation (g_L), thermal generation (g_{th}) and thermal recombination (r_{th}) processes are represented, as well as the position of the quasi-Fermi levels. In (a) the two light generation rates are equal, and in (b) the light generation rate between VB and IB is much higher than that between IB and CB.

The relative strength of the three transitions within the IB material is a sensitive aspect of the IBSC design that needs to be discussed in some detail. It is quite intuitive that the efficiency of the device would sink if part of the energy of the photons gets lost because they are absorbed in a transition of energy lower than possible (for instance, if photons with energy enough to be absorbed in T_{VC} are absorbed in T_{VI}). The most certain way to achieve optimal performance in an IBSC would be then to ensure the selectivity of the absorption coefficients (α_{VC}, α_{VI} and α_{IC}) associated respectively to T_{VC}, T_{VI} and T_{IC}. This implies that α_{IC} should be zero in the range where α_{VI} is non-zero (photon energies $\geq E_H$) and α_{VI} should behave analogously with respect to α_{VC}. But it seems difficult to achieve such a complete selectivity in a real IB material. A more feasible approach is to engineer an IB material with $\alpha_{IC} << \alpha_{VI} << \alpha_{VC}$. It has been proven that this configuration would also lead to optimal efficiencies [3], in particular when assisted by light confinement techniques for the weaker transitions [4]. In the QDs, the optical transition rates depend on the dipole matrix and thereby on the overlapping of the initial and final states involved [5]. This means that the confined-to-confined excitonic transition T_{VI} is stronger than the confined-to-continuum transition T_{IC}. Therefore, the QD material fits well in the $\alpha_{IC} << \alpha_{VI}$ model. The transition T_{VC} associated to the fundamental bandgap is far less problematic in this context. It is reasonably expected to be stronger than the sub-bandgap ones because it is present in the barrier material of the QD stack and also in the emitters, which are much thicker in QD-IBSCs than the IB material.

Let us then forget for the moment the band-to-band transition T_{VC} and focus on the transitions involving the IB. Fig. 1 (a) and (b) show two possible resulting situations when the cell is short-circuited and illuminated only with sub-bandgap photons. In Fig. 1 (a) the generation rates in T_{VI} and T_{IC} are equal, what can be regarded as an optimal situation. Fig. 1 (b) represents the case in which the generation rate associated to T_{VI} is higher than that of T_{IC}. This will be generally the case if the IB is implemented with QDs and no light trapping techniques are used. Fig. 1 (b) represents hence the state-of-the-art situation in QD-IBSC prototypes. In this situation E_{FIB} can be higher than E_{Fe}. We have neglected a possible split between E_{Fe} and E_{Fh}, due to finite mobility which is irrelevant for our discussion and would be small in short-circuit.

The inverted position of E_{FIB} and E_{Fe} that we see in Fig. 1 (b) will necessarily cause a reaction of the system in order to re-establish the population equilibrium. In the same way that in any solar cell a positive E_{Fe} - E_{Fh} split implies the occurrence of recombination, here the negative split between E_{FIB} and E_{Fe} will release thermal generation between the corresponding bands, or as it is commonly said when referring to QDs, thermal escape of carriers from the dots to the CB will be induced.

2 QUANTUM EFFICIENCY EXPERIMENTAL RESULTS AND EQUIVALENT CIRCUIT MODEL

The previous discussion on Fig. 1 (b) will help us to understand the experimental results obtained to the date in QD-IBSC prototypes. The structure and fabrication details of all samples used in this study are very similar to those described in recent works (see for instance [6]). The *IV* characteristics of QD-IBSC prototypes under illumination have been also presented elsewhere [7]. Comparing them to those of GaAs reference samples (samples grown under the same conditions and with the same structure except for not containing the QD layers) we find that they QD-IBSC do not produce significantly more current than their GaAs counterparts.

The I_{SC} produced by different QD-IBSC prototypes depends on the technological details of the QDs growth. The general tendency is that, when very large dots are grown (in order to lower the energy of the confined states and obtain a wider E_L) the strain accumulation causes a poor material quality in the emitter grown on top of the QD stack. For this reason, the I_{SC} of those prototypes is reduced, whereas QD-IBSC prototypes containing stacks of moderate QDs achieve the same current levels of GaAs cells. But in any case, the accumulation of strain in the material always limits the number of QDs layers that can be epitaxially grown. For instance, the samples used in this work contain 10 layers of dots. Thus, the incapability of present QD-IBSC samples to produce significantly more I_{SC} than single gap counterparts is not surprising. To analyze the contribution of the QDs to the photocurrent, more sensitive methods have to be applied. Fig. 2 shows a quantum efficiency (QE) measurement of the QD-IBSCs and here it can be clearly seen that the QDs do produce photocurrent from sub-bandgap photons. From the two absorption thresholds on the graph we can deduce that E_H has in our samples a value around 1 eV and E_L the complementary value of about 0.4 eV (actually closer to 0.3, or even 0.2 eV, if we take into account an undetermined VB offset inherent to InAs/GaAs QDs and/or the states introduced by the wetting layer).

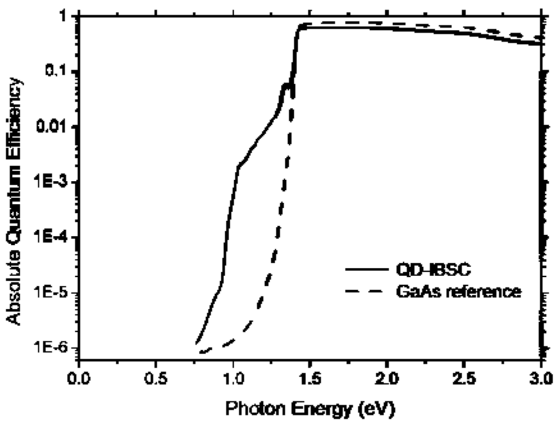

Fig. 2: Room temperature QE of a QD-IBSC prototype and a GaAs reference cell.

We see a sub-bandgap photocurrent in Fig. 2, but from this experiment alone we cannot know its nature. To explain its occurrence, we could consider that the monochromatic photons are being absorbed in both IB transitions according to the IBSC model, but it may also be possible that this photocurrent is better described by the situation of Fig. 1 (b). In fact, it is also possible that through an impact ionization process the absorption of two photons causing transitions from the VB to the IB would lead also to the net generation of an electron-hole pair [10]. In this paper we will focus our discussion on the possibilities that base on light generation processes only, which are expected to be dominant in our system. It might be of interest to study in future works if impact ionization mechanisms make also a significant contribution to the sub-bandgap photocurrent in QD-IBSC prototypes.

Considering the photon energy involved, absorption in T_{IC} implies the transition from a confined state to a continuum state deep in the CB. As it was already mentioned, this kind of transition is far less probable than absorption in T_{VI}, where both final and initial states are localized. Hence, we will assume that the great majority of the photons in this energy range are mainly absorbed in T_{VI} and that the photocurrent is produced through thermal escape from the IB to the CB.

The equivalent circuits represented in Fig. 3 can help us to analyze the QE results. Fig. 3 (a) shows the simplified equivalent circuit of an IBSC under general working conditions. To keep the argumentation straightforward, only simple generation and recombination mechanisms have been taken into account, disregarding Auger processes, shunt resistance, etc (a more complete circuital model can be found in [8]). The current generators labeled $J_{L,XY}$ represent the photogeneration between bands X and Y, while the diodes J_{0XY} represent the recombination between the same bands. Starting from this circuit we can draw the equivalent circuit for our QE measurement in the sub-bandgap range. This is shown in Fig. 3 (b), where it has been assumed that the sub-bandgap photocurrent measured has no contribution of $J_{L,IC}$. Since in a QE measurement the cell is short-circuited, J_{0CV} is not conducting and can be neglected. Regarding the other two recombination diodes, their voltage biases have to compensate each other. This means that when we extract a photocurrent J_R, J_{0IV} is forward biased and J_{0CI} is reverse biased with the same absolute voltage (V_{IV} = -V_{CI}).

The analogy between the circuital model of Fig. 3 (b) and the band diagram of Fig. 1 (b) is straightforward: the negative quasi-Fermi split (E_{FIB} - E_{Fe}) is represented in the model by the reverse bias of J_{0CI} and the thermal generation between IB and CB corresponds to the inverse saturation current of that diode. Given the low value of E_L, the saturation current can be very high at room temperature, not limiting our extraction of J_R for practical values of $J_{L,VI}$ [9]. The split (E_{FIB} - E_{Fh}), which determines the recombination rate between IB and VB,

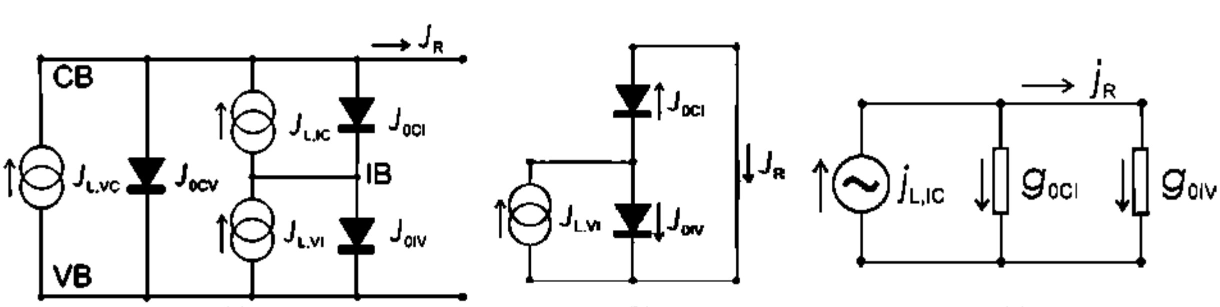

(a) (b) (c)

Fig. 3: Equivalent circuit of the QD-IBSC operation under the different conditions explained in the text: (a) general equivalent circuit, (b) under sub-bandgap continuous illumination (neglecting transitions from the IB to the CB) and short-circuit, and (c) small-signal equivalent circuit for the two-photon absorption experiment.

has its circuit counterpart on the forward bias of J_{0IV}.

If the short-circuit condition is removed, the extraction of sub-bandgap photocurrent through J_{0CI} profiting from thermal escape implies a voltage loss. From the previous argumentation we realize that it is possible to increase the photocurrent of the cell by means of thermal escape, but voltage preservation requires that the absorption of a second photon is feasible to promote electrons from the IB to the CB.

3 TWO-PHOTON ABSORPTION MEASUREMENT

Motivated by the preceding argumentation, we have developed an experimental set-up to test that absorption in T_{IC} does actually take place in QD-IBSCs even if its effect is not strong enough in present prototypes to boost the efficiency. To distinguish the contribution of T_{VI} and T_{IC} to the photocurrent, in our set-up the QD-IBSC is excited simultaneously with two light beams, one of them chopped. A halogen lamp coupled to a monochromator constitutes the primary light source. It provides a monochromatic photon flux that is used to pump electrons from the VB to the IB. The secondary beam comes from a resistive filament that produces light mainly in the IR range. It is filtered by a 350 μm thick GaSb wafer to ensure that no photons from that source with energy over ~ 0.7 eV reach the sample. This implies that the secondary source can only contribute to the T_{IC} transition.

The secondary beam is mechanically chopped at a low frequency and the QD-IBSC is connected to a low noise transresistance preamplifier. The preamplifier has two purposes: it biases the cell at 0 V and converts its photocurrent into a voltage signal. Finally, a lock-in amplifier locked at the chopping frequency measures that ac voltage signal induced by the secondary source. The response to the primary source is a dc photocurrent, analogous to the one measured in a QE experiment (Fig. 2) and it is not recorded by the lock-in.

When we apply this experimental procedure to our QD-IBSC prototypes, we do not extract ac signal at room temperature. But this does not necessarily imply that there is no absorption in the T_{IC} transition. This will become clear again with the help of the circuital model.

Given the small absorption provided by the QDs for the T_{IC} transition, we can assume in our set-up that $j_{L,IC}$ behaves as a small signal superposed to the polarization dc current $J_{L,VI}$ for any excitation intensity. Fig. 3 (c) is the equivalent small-signal circuit for the secondary excitation, where g_{0CI} and g_{0IV} represent the respective small signal conductances of J_{0CI} and J_{0IV}. The value of these conductances is determined by the bias circuit represented in Fig. 3 (b). The possibility of extracting a measurable ac signal photocurrent j_R will depend on the ratio of both conductances. Although J_{0CI} is reverse biased and J_{0IV} forward biased, the small value of E_L compared to E_H, and the subsequent high saturation current, can make g_{0CI} much higher than g_{0IV}, reducing j_R to values below the detection limit of our set-up. Put in other words, if the thermal escape from the IB to the CB is very efficient in letting $J_{L,IV}$ flow to the contacts, we will see no difference when activating $j_{L,IC}$. The hypothesis of our experiment is that by lowering the temperature of the device we can reduce g_{0CI} to a level at which, if $j_{L,IC}$ is actually active, we will be able to measure a corresponding photocurrent signal.

4 EXPERIMENTAL RESULTS

Fig. 4 shows the photocurrent measured with the described set-up for different temperatures of the cell at a fixed wavelength of the primary source. To lower temperature, the QD-IBSC has been placed in a closed-cycle He-cryostat. It can be seen that for temperatures lower than 100K the photocurrent signal raises over the noise level, reaching its maximum at about 40K.

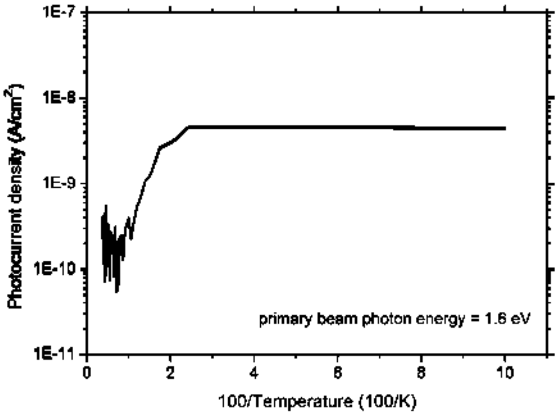

Fig. 4: Dependence of the measured two-photon photocurrent on the temperature.

The photocurrent showed in Fig. 4 is a direct proof of the existence of non-zero $j_{L,IC}$, which is directly associated to the generation of current due to transitions from the IB to the CB as we wanted to demonstrate. Let us now analyze, continuing with the circuital model, how the temperature decrease has enabled its extraction. The measured signal can be written as

$$j_R = \frac{j_{L,IC}}{1 + g_{0CI}/g_{0IV}} \tag{1}$$

Let us assume, to simplify the discussion, that J_{0CI} and J_{0IV} can be modelled as ideal diodes and that the variation of the respective bandgaps with the temperature is negligible. In the low-frequency regime the conductances are independent of the frequency and take the form [11]

$$g_{0XY} = J^0_{0XY}\frac{q}{kT}\exp(qV_{XY}/kT) \tag{2}$$

where q and k stand as usual for electron charge and Boltzmann constant, and J^0_{0XY} represents the reverse saturation current of diode J_{0XY}. The reverse saturation current of an ideal diode is proportional to $(n_i)^2$, being n_i the intrinsic concentration at that temperature. The proportionally factor is determined by the electrical properties of the carrier that contributes more to the current flow (in a p^+n junction, for instance, it would be the holes). In g_{0CI} this factor is determined by the properties of CB electrons, and in g_{0IV} by those of VB holes. As the dependence of these factors on the temperature, as well as the dependence of the effective densities of states, is not significantly different for both diodes, we can write

$$\frac{g_{0CI}}{g_{0IV}} \propto \frac{n^2_{i,IC}\exp\left(\frac{qV_{CI}}{kT}\right)}{n^2_{i,VI}\exp\left(\frac{qV_{IV}}{kT}\right)} \propto \exp\left(\frac{(E_H - E_L) - 2qV_{IV}}{kT}\right) \tag{3}$$

The first term in (3) comes from the saturation currents and depends on the difference between both bandgaps. The higher the difference, the higher the g_{0CI}/g_{0IV} ratio, and if this term is dominant, decreasing T would only increase it, making the extraction of j_R even more difficult. The second term comes from the biasing of the diodes. If the voltage drop induced by $J_{L,VI}$ is sufficiently high (in our case about 0.35 V), this term becomes dominant. Substituting expression (3) in (2) for this case agrees with the result of Fig. 4. It must be also taken into account that when T decreases and both saturation currents are reduced, V_{IV} necessarily increases to allow the dc current flow in both diodes. For $T \rightarrow 0$ both saturation currents approach zero, that means that thermal escape between IB and CB is suppressed and diode J_{0IV} is in open-circuit, with a voltage drop approaching E_H/q.

On the other hand, expression (2) has been derived from the ideal diode model. Introduction of non idealities, such as traps, would affect more diode J_{0CI} than J_{0IV} (it must be remembered that real QDs introduce more than one confined level). Another probable current contribution would be that produced by tunnel escape of carriers from the dots. In our circuital model this mechanism would act as a low value shunt resistance affecting also J_{0CI}. All these mechanisms, that swell g_{0CI} at room temperature, are strongly inhibited when T is decreased and would also justify the observed dependence of g_{0CI}/g_{0IV} on T even for lower V_{IV} values as deduced from (3).

Coming back to the experimental results, Fig. 5 shows the two-photon photocurrent j_R versus the photon energy of the primary source, measured at different temperatures. The dashed line represents the dc photocurrent J_R induced by the primary light at the highest temperature (actually this curve has been measured switching off the secondary source and chopping the primary source, and then corrected with the corresponding factor $\sqrt{2}$). The curve marked with solid squares corresponds to the noise level of the experiment, also at 80K. It is the j_R recorded when the secondary source is switched off.

Fig. 6 shows the photocurrent measurements for a fixed T of 6K and different intensities of both light sources. Again, it contains two types of measurement: solid lines (curves (2), (3) and (5)) are two-photon photocurrent j_R, whereas the two dashed lines ((1) and (4)) represent the dc photocurrent J_R. Curves (1) and (2) correspond to J_R and j_R for a given power of the light sources ($J_{L,IV}$ high, $j_{L,IC}$ high). Curve (3) resulted from lowering the intensity of the secondary source while maintaining that of the primary source ($J_{L,IV}$ high, $j_{L,IC}$ low). Finally, curves (4) and (5) correspond to J_R and j_R when the original intensity is maintained in the secondary source and the power of the primary source is lowered ($J_{L,IV}$ low, $j_{L,IC}$ high). The slight differences in the shape of the curves between both graphs come from compositional details of the QD-IBSC samples used that are not relevant for this discussion. It must be remarked that these photocurrent measurements are not normalized as the absolute QE of Fig. 2 was. Their shape is conditioned by the spectral distribution of the primary source in each experiment.

From Figs. 5 and 6 it is noticed that the two-photon experiment will give a positive result not only when the wavelength of the primary source is in the sub-bandgap range (actually, Fig. 4 showed also the photocurrent measured when the photon energy of the primary source is 1.6 eV). Although J_R is very large over E_G, the majority of the photons are absorbed in T_{CV} and the contribution to $J_{L,VI}$ is small. As the energy of those photons decreases, the possibility of not being absorbed in the emitter and reaching the dots is higher. It must be remembered though that even very energetic photons, which are completely absorbed near the surface of the device, can reach the dots and be reabsorbed by them through photon recycling.

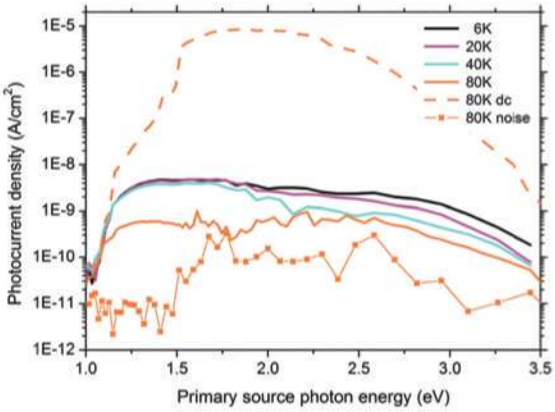

Fig. 5: Dependence of the two-photon photocurrent on the primary source photon energy for different temperatures.

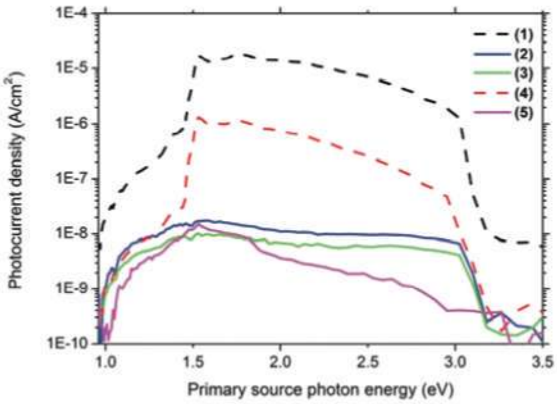

Fig. 6: Dependence of the two-photon photocurrent on the primary source photon energy for different primary and secondary light intensities. All measurement taken at 6K.

The measurements showed in Figs. 5 and 6 agree with the circuital model of the QD-IBSC exposed. There is no signal j_R if there is no absorption in T_{IV} (the diodes are at 0V and g_{0CI} is much higher than g_{0IV} for any T). In the range of Fig. 5 where $J_{L,IV}$ is higher, the signal has already saturated at 40K, whereas in the range of lower $J_{L,IV}$ it has not (the 80K curve shows a different behaviour, but this is due to the low signal to noise ratio at that temperature, as it can be seen by comparison to the noise level curve). Regarding Fig. 6, comparison between curve (2) and (3) shows that j_R is proportional to $j_{L,IC}$ for any value of $J_{L,IV}$, as predicted by eq. (1). When the intensity of the primary source is low, the induced

$J_{L,IV}$ and V_{IV} are small, and j_R is very sensitive to their changes. That is the case of curve (5). But when $J_{L,IV}$ is much higher, expression (3) becomes ~ 1 and j_R almost saturates, as showed by curves (2) and (3).

5 CONCLUSIONS AND FUTURE PROSPECTS

The absorption of sub-bandgap photons in the transition between the IB and CB in QD-IBSC prototypes and subsequent production of photocurrent has been experimentally proven. Comparison with an equivalent circuit model shows that the experimental results are in agreement with the theoretical principles of the IBSC. It is concluded from this analysis that the addition of this absorption to the absorption between VB and IB produces photocurrent, but this photocurrent cannot be measured at room temperature for two reasons: first, the absorption between IB and CB is very small in present devices, and second, the escape of carriers from the IB to the CB is too high. Lowering the temperature of the device has removed the second impediment and enabled the extraction of that photocurrent.

Once it has been demonstrated that absorption in both sub-bandgap transitions and subsequent production of photocurrent does actually take place in QD-IBSCs, technological improvements have to be undertaken to promote this effect. From the results obtained to the date, the main short-term goals seem to be: (a) to enhance the absorption in the sub-bandgap range (growing more QD layers and/or implementing IR light trapping techniques), (b) to optimize the dot size, in order to increase the bandgap between IB and CB and reduce the thermal escape and recombination between these bands and (c) to improve the overall material quality, included the emitter grown on top of the dots. From a technological point of view, the achievement of these objectives is much related to the capability of controlling strain accumulation. At this respect, notable improvements have been recently attained. Hubbard et al. [12] have grown QD-IBSCs of excellent material quality through insertion of GaP strain-relief layers between QD layers. Using another strain-relief strategy, the substitution of GaAs by InP (substrate) and InGaAlAs (barrier material), Oshima et al. have grown stacks of 100 QD layers of high uniformity [13]. The goal would be then to apply such strategies to obtain QD-IBSCs with thicker stacks and dots of optimized size.

To optimize the dot size it must be taken into account that there is a trade-off between the position of the IB and the number of extra confined levels. If large dots are grown, the ground state is low, but a high number of levels would be introduced between IB and CB, adding new recombination paths and consequently lowering the efficiency. From the theoretical model it is expected that at high illumination intensities these recombination paths saturate and the direct transitions between bands dominate [14]. This means that at high light concentrations the effect of extra levels is minimized and the efficiencies expected for the IBSC of three isolated bands are recovered. The higher the concentration ratio, the higher the number of extra levels that can be tolerated. So, if a compromise between dot size and practical concentration ratios is found, it is expected that the strategy described before, together with the use of light concentration, lead to the improvement of QD-IBSC performances.

6 ACKNOWLEDGMENTS

This work has been supported by the project FULLSPECTRUM, funded by the European Commission under Contract No. SES6-CT-2003-502620, the Spanish Plan for R&D Consolider-GENESIS FV (CSD2006-0004) and the Comunidad de Madrid Program NUMANCIA (S-0505/ENE/000310). E.A. and P.G.L acknowledge the UPM grant program. D.F.M acknowledges financial support from the Spanish Ministry of Science and Innovation within the program Ramón y Cajal.

7 REFERENCES

[1] A. Luque, and A. Martí, Physical Review Letters **78**, 5014 (1997).
[2] A. Martí, L. Cuadra, and A. Luque, in *Proc. of the 28th IEEE Photovoltaics Specialists Conference*, edited by IEEE New York, 2000), pp. 904.
[3] L. Cuadra, A. Martí, and A. Luque, IEEE Transactions on Electron Devices **51**, 1002 (2004).
[4] A. Martí *et al.*, in MRS Proceedings, Spring Meeting 2008, San Francisco, vol. 1101E, pp. KK06-02.
[5] M. Sugawara, *Self-assembled InGaAs/GaAs quantum dots* (Academic Press, 1999), Vol. 60.
[6] A. Martí *et al.*, Physical Review Letters **97**, 247701 (2006).
[7] A. Luque *et al.*, Journal of Applied Physics **99**, 094503 (2006).
[8] A. Luque *et al.*, J. Appl. Phys. **96**, 903 (2004).
[9] A. Martí, C. R. Stanley, and A. Luque, *in T. Soga (Ed.), Nanostructured Materials for Solar Energy Conversion, Chap 17* (Elsevier, 2006).
[10] A. Luque, A. Martí, and L. Cuadra, IEEE Transactions on Electron Devices **50**, 447 (2003).
[11] G. W. Neudeck, *The pn junction diode* (Addison-Wesley Publishing Company, Vol. II.
[12] S. M. Hubbard *et al.*, Appl. Phys. Lett. **92**, 123512 (2008).
[13] R. Oshima *et al.*, Journal of Crystal Growth **301-302**, 776 (2007).
[14] A. Martí *et al.*, Thin Solid Films (2007).